

1 **Supplementary Information**

2 **Rhodospseudomonas Palustris Based Conversion of Organic** 3 **Acids to Hydrogen Using Plasmonic Nanoparticles and Near-** 4 **Infrared Light**

5 John Craven^a, Mansoor A. Sultan^b, Rupam Sarma^a, Sarah Wilson^a, Noah Meeks^d,
6 Doo Young Kim^c, J. Todd Hastings^b, Dibakar Bhattacharyya^{*a}

7 ^a Department of Chemical and Materials Engineering, University of Kentucky, Lexington, KY
8 40506

9 ^b Department of Electrical and Computer Engineering, University of Kentucky, Lexington, KY
10 40506

11 ^c Department of Chemistry, University of Kentucky, Lexington, KY 40506

12 ^d Southern Company Services, Inc., Birmingham, AL 35203

13 **Growth in various media**

14 *R. Palustris* (CGA 009) cultures were grown using various media types at the outset of the project
15 to select growth conditions for further experiments. Complex media types suggested by ATCC ¹ provide a
16 rich media for growth of precultures, but preclude certainty in the molecular source of carbon and
17 nitrogen due to the use of yeast extract or soy broth. Defined media types are used either to control the
18 specific nutrients used by microbes or as a means of limiting contamination. Further for metabolically
19 versatile organisms like *R. Palustris* the media content determines not only the efficacy of growth, but
20 whether or not the organism grows in a phototrophic / chemotrophic or heterotrophic / autotrophic
21 domain. Complex media types with excess fixed nitrogen in particular are useful for pregrowth of
22 bacterial cultures, but this fixed nitrogen content results in downregulation of nitrogenase activity
23 required for hydrogen production.

24 Growth from various media types is shown in **Supplementary Figure 1a** for cultures illuminated
25 with white LED, and in **Supplementary Figure 1b** for cultures grown in the dark. Complex media types
26 1 and 2 resulted in the shortest lag phase, which was expected for rich complex cultures. Complex type 3
27 showed little growth, likely due to low concentration (0.2 g/L) of yeast extract. Both defined media types
28 showed increased lag phase, but Defined 1, which was chosen for hydrogen production experiments,
29 resulted in a higher cell density. Notably only complex media types 1 and 2 showed significant growth
30 without illumination, indicating that these media types were able to sustain chemotrophic growth.

31

32

33 **Supplementary Table 1: Media Recipes.** Complex and defined media recipes used for bacterial growth.

Component (g/L)	Complex 1¹	Complex 2¹	Complex 3³	Defined 1⁴	Defined 2⁵
Sodium Acetate			2.74	5.74	5.74
Sodium Glutamate				1.18	1.18
Tryptic Soy Broth	15				
Yeast Extract		10	0.2		
K ₂ HPO ₄		1			
MgSO ₄		0.5		0.12	0.24
L-cysteine		0.6			
NH ₄ Cl			0.65		1
Na ₂ HPO ₄				6.8	6.9
KH ₂ PO ₄				3	3
NaCl				0.58	0.5
(NH ₄) ₂ SO ₄				1.32	
CaCl ₂ •2H ₂ O				0.1 mM	0.015
Thiamine HCl				1 mg/L	
Trace Metals Stock				10 mL/L	

34

35

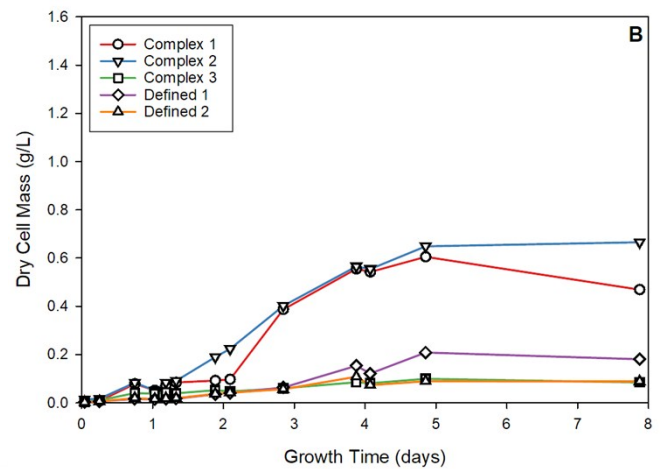
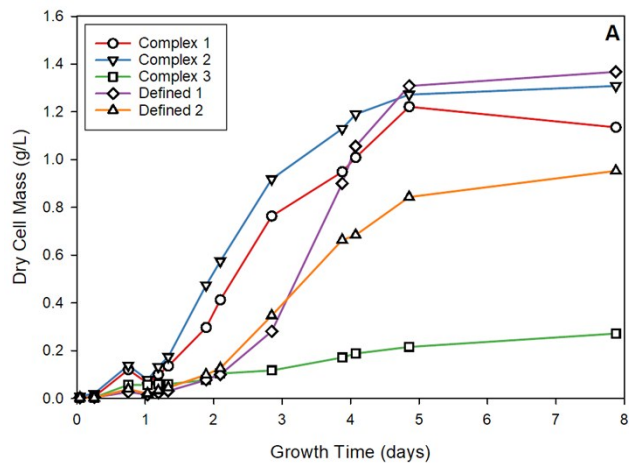
36

37 **Supplementary Table 2: Trace Metals Stock.** Used in Defined media 1.

Trace Metals Stock (g/L)	
CaCl ₂ •2H ₂ O	0.729
FeCl ₃ •6H ₂ O	1.666
MnCl ₂	0.064
ZnCl ₂	0.170
CuCl ₂ •2H ₂ O	0.043
CoCl•6H ₂ O	0.060
Na ₂ MoO ₄ •2H ₂ O	0.060

38

39



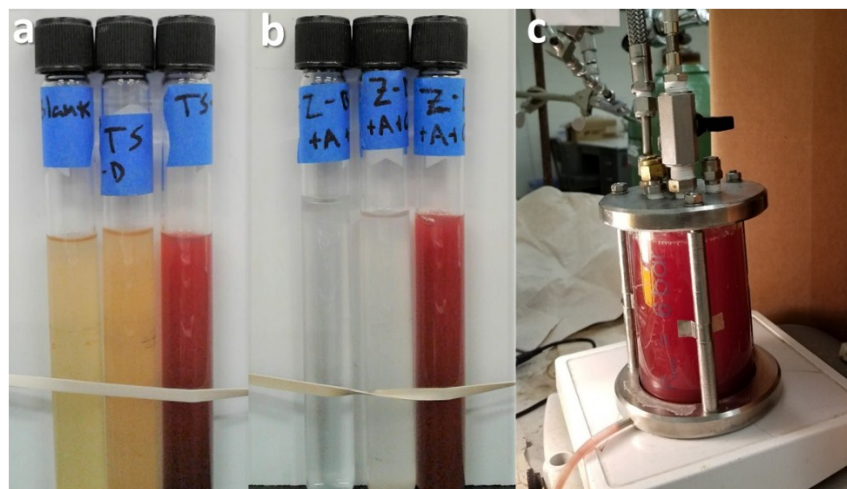
40

41 **Supplementary Figure 1: *R. Palustris* growth in various media.** Anaerobic growth of *R. palustris* in 20mL sealed
 42 test tubes media at 30 °C. Media recipes are shown in **Supplement Table 1,2** **A)** Samples grown under white LED
 43 (20 W/m²) illumination. **B)** Samples grown in the dark, covered in aluminum foil.

44

45 **Bacteria Pigmentation**

46 Development of bacteriochlorophyll in *R. Palustris* from phototrophic growth results in dark red
 47 pigmentation shown below for both complex and minimal media.



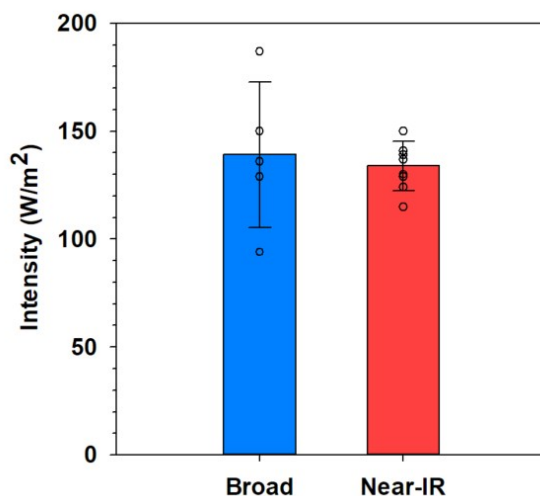
Supplementary Figure 2: Pigmentation of *R. Palustris*. a,b) Vials of media inoculated from left to right; blank media, inoculated media grown under anaerobic dark conditions, inoculated media grown under anaerobic light conditions with 2500 lumens white LED. a) Soy based media b) minimal media using 70mM acetate and 7mM glutamate as carbon and nitrogen sources. c) 300mL reactor growing *R. Palustris* exhibiting strong pigmentation.

48

49

50 Light Intensity

51 For batch experiments comparing two light sources, the maximum intensity of the two
52 sources was adjusted to be equal using a calibrated detector as shown in **Supplementary Figure**
53 **3b**. Differences in the dispersion of light from these sources resulted in a higher variance from
54 the simple tungsten bulb than from the near-IR LED array, shown below. Vials were shaken on
55 their sides and illuminated from the flat vial bottom. Each intensity measurement represents the
56 intensity at the surface of one of the vials.



Supplementary Figure 3: Intensity comparison for using two light sources to illuminate 40mL septa vials from the bottom. Intensity measured at the middle of each vial normal to the vial surface.

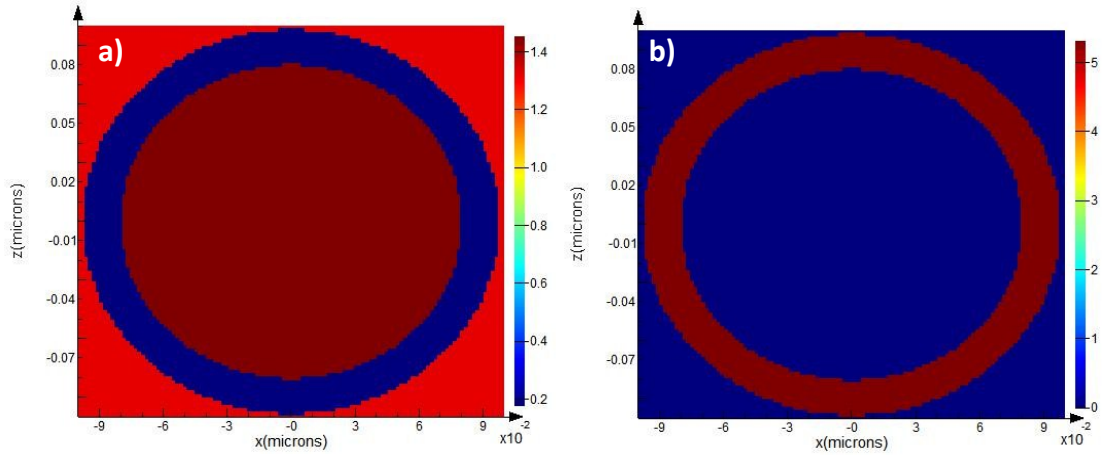
57

58

59 Numerical Simulation and Characterization of Nanoparticles

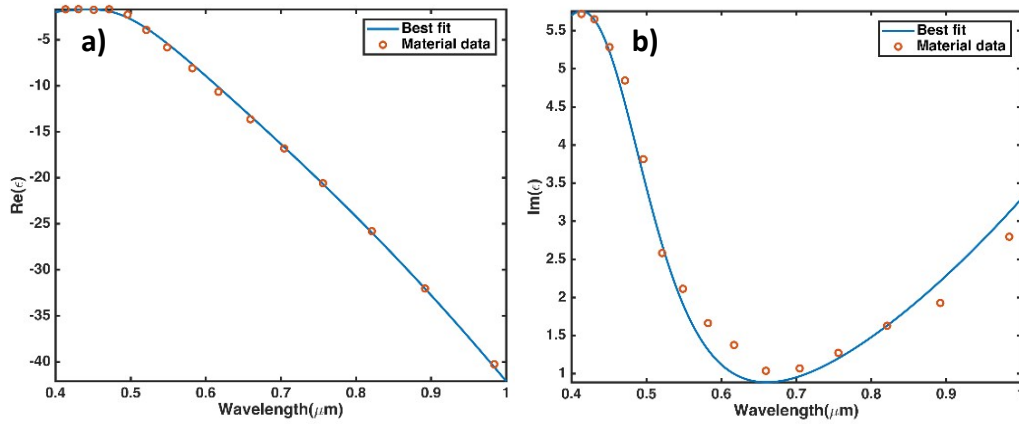
60 In order to find the particles with best match of extinction cross section with *R. Palustris*,
61 numerical analysis for particles geometry and material was implemented. Finite different time
62 domain analysis (Lumerical Inc.) was utilized to simulate the suspended particles in water to
63 estimate the resonance wavelength, scattering cross section, absorption cross section, and electric
64 field enhancement. **Supplementary Figure 4** shows a cross section through a particle with the
65 resonance matched to the bacteriochlorophyll absorption peak at 850 nm. The figure maps the
66 real and imaginary part of the refractive index at $\lambda = 850 \text{ nm}$. The refractive index for gold was
67 taken from Johnson & Christy² and the refractive indices for water and silica were taken from
68 Palik⁶. The best fit models for the material properties are shown in **Supplementary Figures 5**
69 **and 6**. The full mathematical modeling of electromagnetic wave scattering in core-shell
70 particles has been reported in the literature⁷. The calculated absorption, scattering and extinction
71 cross sections are shown in **Supplementary Figure 7**.

72



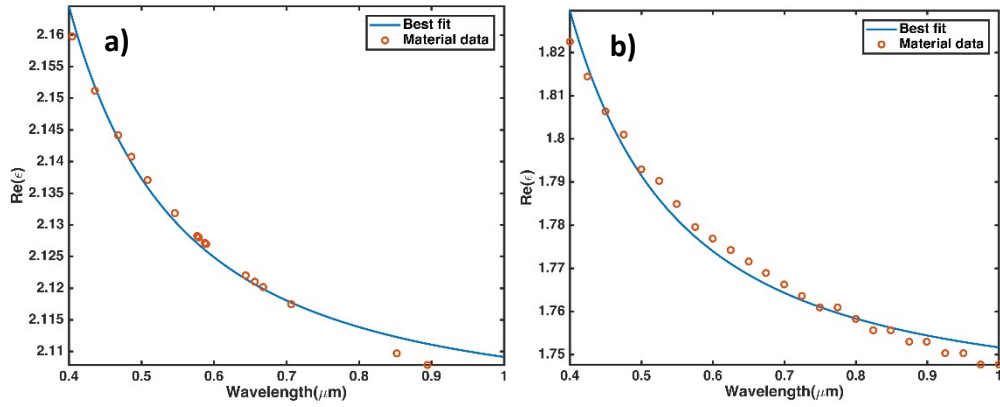
Supplementary Figure 4: Refractive index map used for simulation. a) Real part and b) Imaginary part of refractive index at $\lambda = 850$ nm.

73



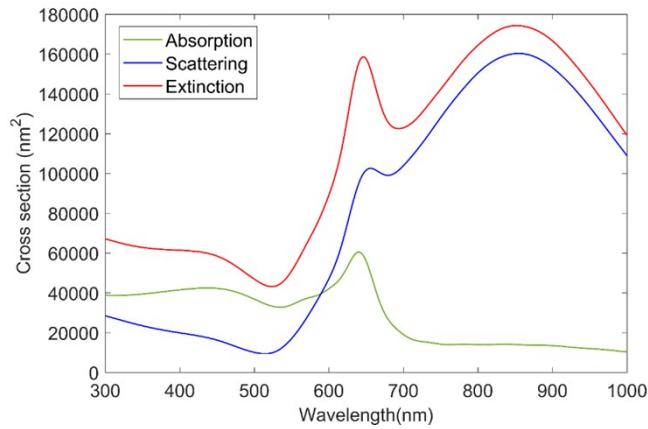
Supplementary Figure 5: Best fit for dielectric constant of gold based on Johnson and Christy ². a) Real part and b) imaginary part.

74



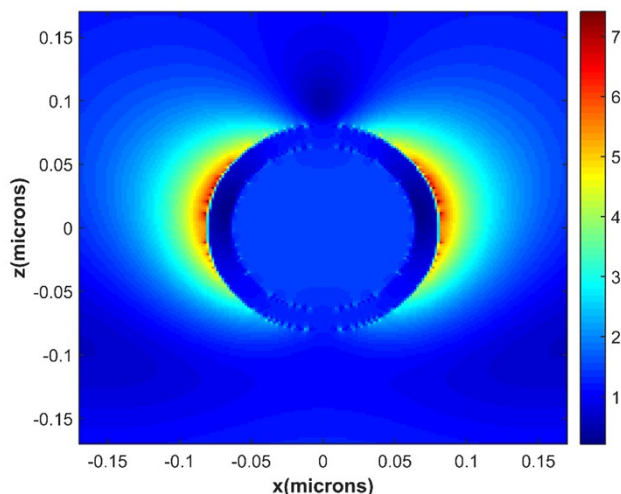
Supplementary Figure 6: Best fit for real part dielectric constant of SiO_2 and water based on Palik for (a) SiO_2 and (b) water.

75



Supplementary Figure 7: FDTD simulation results for optimum silica-gold core-shell particles with resonance wavelength at 850 nm. The extinction cross section represents the sum of absorption and scattering. The diameter of the core is 120 nm and thickness of shell is 18nm.

76

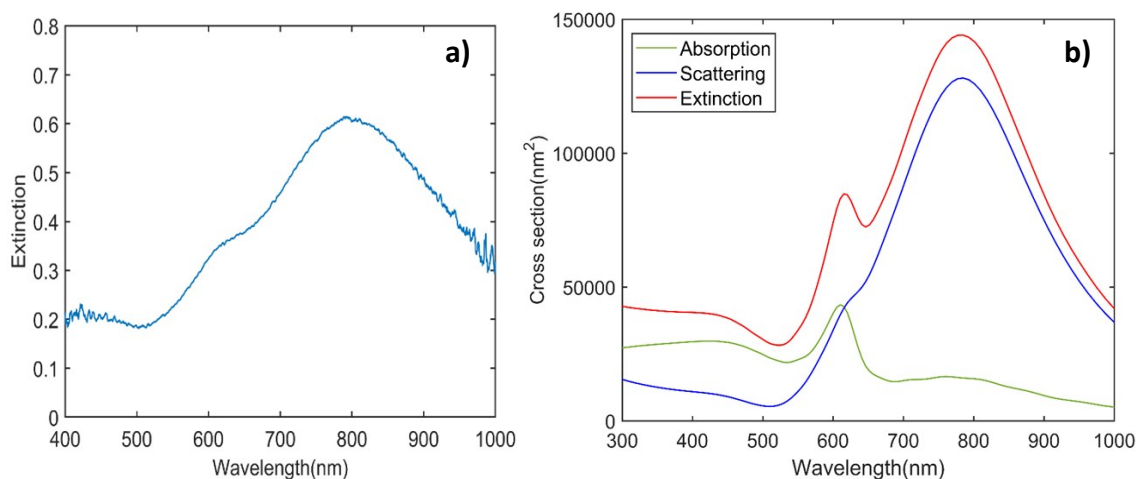


Supplementary Figure 8: Electric field profile around the silica-core gold shell particle calculated at $\lambda = 850$ nm. The light is propagating along the z-axis with linear polarized electric field along the x-axis.

77

78 The field profile around the particle is shown in **Supplementary Figure 8** and it can be
79 seen that the field is enhanced 7 times around the particle over a distance of ~ 30 nm

80 Commercially available water suspensions of silica-core gold nanoshells with a
81 resonance wavelength of 800 nm were purchased from NanoCompsix. The core diameter of
82 these particles is 120 ± 9 nm and the shell thickness is 16 nm. These shells were coated poly
83 (ethylene glycol) methyl ether (mPEG). The extinction spectrum of these particles was measured
84 using an Ocean Optics HR4000CG-UV-NIR spectrophotometer and are shown along with FDTD
85 simulations in **Supplementary Figure 9**. The resonance is centered at 800nm in both cases.



Supplementary Figure 9: **a)** Extinction spectrum for purchased particles. **b)** FDTD simulation for purchased particles. The match between simulation and absorption spectrum can be noticed at 800 nm which represents the resonance wavelength for these particles.

86

87

88 Temperature Variance and Hydrogen Production

89 The gold-silica core-shell nanoparticles used in the manuscript absorb light in the visible
90 and near-infrared range. A series of experiments and calculations were performed to determine
91 the increase in the bulk media temperature due to the addition of nanoparticles, and the impact of
92 increased temperature on hydrogen production from *R. palustris*. Briefly, these results showed
93 that the presence of nanoparticles at the experimental concentration in media alone resulted in a
94 small temperature increase (<1 °C), which agrees with theoretical calculations shown below.
95 Additionally, an experiment was performed without the addition of nanoparticles using NIR
96 illumination at two temperatures (25 and 40 °C) found that cultures held at 40 °C resulted in
97 decreased hydrogen production. This result agrees with the work of Wang et al. who found that
98 hydrogen production from *R. palustris* cultures illuminated with visible LEDs was maximized
99 around 30 °C and that further temperature increase was detrimental⁸.

100 The maximum generated heat will happen at the maximum absorption cross-section that
101 associated with wavelength of ~600 nm which is out of the used LED emission spectrum. To
102 calculate the highest total steady state heating power due to absorption, it was assumed that the
103 particle is uniform gold sphere instead of shell to calculate for the worst case scenario.

$$104 \quad Q = \sigma_{abs} I_0 \quad (1)$$

105 Where σ_{abs} is the calculated absorption cross-section of the used particle
106 ($= 1.445 \times 10^{-14} m^2$) at 850 nm and I_0 is the light intensity of LED ($=130 W/m^2$). The
107 maximum temperature increase of particle will be

$$108 \quad \Delta T = \frac{Q}{4\pi R_{eq} \kappa_{water}} \quad (2)$$

109 For spherical structure R_{eq} will be equal to the radius of particle ($= 80$ nm) and κ_{water} is
110 Thermal conductivity of water $= 0.58 (K/Wm^{-1}K^{-1})$.

111 Calculating ΔT from equation (2) we obtain maximum temperature increase as

$$112 \quad \Delta T = 3.22 \times 10^{-6} K$$

113 Which means there is no significant heat change around particles of this dimensions with
114 this wavelength and that agrees with finding of Harris et al.⁹ where they found that core-shell
115 particles immersed in water will not have a noticeable temperature increment.

116 To confirm our calculations for temperature rise due to the presence of NP, two
117 measurements were obtained from two samples under NIR illumination. The steady state
118 temperatures of NIR illuminated vials of water or in nanoparticle solution at the same
119 concentration used in the experiments presented in the manuscript (2.6×10^8 particles/mL) were
120 measured over the course of 3 days while shaking in an incubator without temperature control.
121 The differences in temperature at steady state were less than 1 °C as shown below.

122

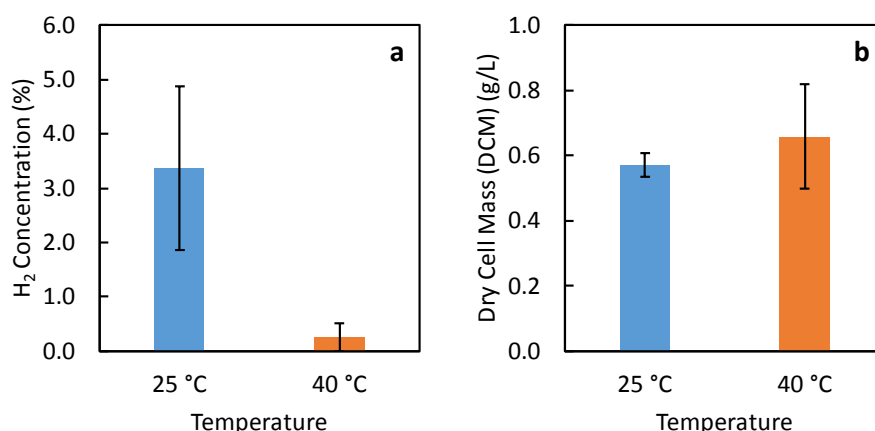
123 **Supplementary Table 3:** Temperature increase in media with and without gold-silica core-shell nanoparticles

	Temperature (°C)
<hr/>	
DI	
Water	27.5 ± 0.1
NP	
Solution	28.2 ± 0.1
<hr/>	
Diff	
erence	0.8 ± 0.1

124

125 In order to test the effect of elevated temperature on hydrogen production of *R. Palustris*
126 we incubated 5 vials at without temperature control, around 25 °C, and 5 vials with temperature
127 control at 40 °C. Each 40mL vial was inoculated at a high cell concentration of 0.6 g/L and
128 illuminated with NIR LED array. After 24 hours growth the headspace was measured for
129 hydrogen concentration and the culture was tested for cell concentration using optical density at
130 660nm, shown below. The cultures at 25 °C produced roughly 10x the amount of hydrogen as
131 those cultures held at 40 °C from comparable cell densities. The high degree of variance in this
132 experiment is likely due to a short incubation time and high inoculation concentration which
133 magnified variance in cell viability between the cultures. This is consistent with the results of
134 Wang et al⁸ who conducted visible light illumination studies with *R. palustris*, that the optimum
135 temperature for hydrogen production was 30 °C and dropped significantly at 40 °C.

136



137

138 **Supplementary Figure 10:** Hydrogen production at two temperatures. 40mL vials filled with 30mL
139 minimal media were inoculated at an initial DCM of 0.6 g/L, and illuminated at the designated temperature for 24
140 hours using NIR LED arrays. **a)** hydrogen produced over the course of the experiment **b)** final dry cell mass of the
141 cultures after 24 hours calculated from optical density at 660 nm.

142

143 **References**

- 144 1. Rhodopseudomonas palustris (Molisch) van Niel ATCC® BAA-98™).
- 145 2. P. B. Johnson and R.-W. Christy, *Physical Review B*, 1972, **6**, 4370-4379.
- 146 3. P. Carlozzi and A. Sacchi, *Journal of Biotechnology*, 2001, **88**, 239-249.
- 147 4. J. Zhao, T. Baba, H. Mori and K. Shimizu, *Metabolic Engineering*, 2004, **6**, 164-174.
- 148 5. Y.-C. Liao, T.-W. Huang, F.-C. Chen, P. Charusanti, J. S. J. Hong, H.-Y. Chang, S.-F. Tsai, B. O.
- 149 Palsson and C. A. Hsiung, *Journal of Bacteriology*, 2011, **193**, 1710-1717.
- 150 6. E. D. Palik, *Handbook of optical constants of solids*, 1985.
- 151 7. A. L. Aden and M. Kerker, *Journal of Applied Physics*, 1951, **22**, 1242-1246.
- 152 8. Y.-Z. Wang, Q. Liao, X. Zhu, X. Tian and C. Zhang, *Bioresource Technology*, 2010, **101**, 4034-4041.
- 153 9. N. Harris, M. J. Ford and M. B. Cortie, *The Journal of Physical Chemistry B*, 2006, **110**, 10701-
- 154 10707.

155